Check for updates

Fabrication of Smooth, Periodic Surface Structures: Combining Direct Laser Interference Patterning and Electropolishing

Christian Schäfer, Pablo Maria Delfino, Philipp Leonhard-Trautmann, Vincent Ott, Sebastian Suarez, Michael Stüber, Frank Mücklich, and Christoph Pauly*

The manipulation of topography is crucial in surface engineering to customize material properties and surface functionalities for specific applications. Scientists have been inspired by natural surfaces found in plants and animals and have increasingly used engineered surface structures to improve characteristics such as friction, wear, electrical resistance, wettability, and antimicrobial behavior across various fields. Direct laser interference patterning (DLIP) is a technique that can rapidly create well-defined, periodic surface structures. However, it can still face challenges such as surface roughness and non-uniformity, which require complementary post-processing techniques. This article investigates the effectiveness of electropolishing in phosphoric acid as a post-processing method for DLIP-treated copper surfaces. Through systematic characterization and analysis, it is demonstrated that electropolishing selectively smoothens DLIP-treated surfaces by removing undesired by-products, such as oxides and redeposited material while retaining the underlying structure. The real surface area and, consequently, the *S* ratio are diminished by up to 13%, while the root mean square roughness R_q along the topographic maxima of the line pattern is reduced by ≈90%. These findings contribute to the advancement of our understanding of surface modification techniques and their potential applications in diverse fields.

1. Introduction

The controlled manipulation of the surface topography plays a pivotal role in surface engineering, tailoring the material's properties to the requirements of the aimed field of application. In nature, many plants and animals have well-defined, ordered surface structures that fulfill very specific functions based on several thousand years of evolution.[1] In recent years, more and more scientists have used the advantageous properties of such surfaces as a template and transferred them to technical components. The benefits of engineered surface structures extend across a wide spectrum of fields by providing control over certain characteristics such as friction and wear in tribological systems,[2–4] electrical resistance,[5] insertion forces and fretting behavior in electrical systems,[6,7] wettability,[8–11] solar cell efficiency,[12,13] antimicrobial behavior,[14,15] biological cell adhesion,[16,17] and decorative or diffractive properties for protection against counterfeit.[18,19]

Several approaches have been explored to create such structures, ranging from traditional methods like mechanical milling,[20] micro-coining,[21] burnishing,[22] honing,[23] lithography and chemical etching,[24] to more sophisticated laser-based techniques such as direct laser writing (DLW) or DLIP.[25,26] Among these, DLIP has emerged as a superior candidate, offering a rapid, reproducible, and highly controllable means of producing well-defined, periodic surface structures. This technique harnesses the interference patterns of multiple laser beams to induce a periodic modulation, providing a versatile and scalable approach for surface engineering.[27]

C. Schäfer, P. M. Delfino, P. Leonhard-Trautmann, S. Suarez, F. Mücklich, C. Pauly
Chair of Functional Materials
Saarland University
Campus D3.3, 66123 Saarbrücken, Germany
E-mail: christian.schaefer@uni-saarland.de

The ORCID identification number(s) for the author(s) of this article can be found under https://doi.org/10.1002/adem.202400435.

© 2024 The Author(s). Advanced Engineering Materials published by Wiley-VCH GmbH. This is an open access article under the terms of the Creative Commons Attribution-NonCommercial-NoDerivs License, which permits use and distribution in any medium, provided the original work is properly cited, the use is non-commercial and no modifications or adaptations are made.

DOI: 10.1002/adem.202400435

P. M. Delfino
Advanced Instrumentation for Nano-Analytics (AINA)
Luxembourg Institute of Science and Technology
41 rue du Brill, L-4422 Belvaux, Luxembourg

V. Ott, M. Stüber
Angewandte Werkstoffphysik (IAM-AWP)
Karlsruher Institut für Technologie (KIT)
Hermann-von-Helmholtz-Platz 1, 76344 Eggenstein-Leopoldshafen, Germany

15272648, 2025, 3, Downloaded from https://advanced.onlinelibrary.wiley.com/doi/10.1002/adem.202400435 by Universitätsbibliothek der Universität des Saarlandes, Wiley Online Library on [14/03/2025]. See the Terms and Conditions (https://onlinelibrary.wiley.com/terms-and-conditions) on Wiley Online Library for rules of use; OA articles are governed by the applicable Creative Commons License

While DLIP exhibits promising advantages, there remains a pressing need for further refinement and enhancement of these surface structures depending on the application. Challenges such as surface roughness and non-uniformity on a sub-wavelength scale persist, prompting the exploration of complementary post-processing techniques. Laser processing of metals usually results in the formation of oxides and redeposited material, primarily on the topographical maxima of the pattern. Moreover, laser-induced periodic surface structures (LIPSS) can be produced through the interference between the incident laser beam and electromagnetic waves.[28] These waves are initiated by the excitation of surface plasmon-polaritons on metals when utilizing ultrashort pulsed laser sources.[29] In the case of strongly absorbing materials like metals, low-spatial-frequency LIPSS often emerge, characterized by a structure period close to the laser wavelength and an orientation perpendicular to the beam polarization.[30] Conversely, transparent materials predominantly exhibit high-spatial-frequency LIPSS with significantly smaller periods.[31–33]

In tribological systems, as a consequence of the superimposed surface roughness, sharp asperities protruding from the contact area plastically deform due to high local contact pressures or get worn off during the run-in between the contacting surfaces. Upon continuous tribological exposure, those wear particles may significantly increase the abrasive component of the tribological system.[25] Another important field in which DLIP-derived consequences might play a detrimental role are electrical contacts. In this case, it is well known that contaminants and low-order irregularities increase the electrical contact resistance, resulting in Joule heating losses at the interface, compromising their proper function and reducing the operational life of components.[34]

In the field of physical vapor deposition (PVD), substrate surface irregularities and particle contaminations are a notorious source of layer defects caused by shadowing effects during the deposition process.[35] For instance, rough surfaces and sharp asperities protruding from the substrate's surface can result in the formation of non-uniformly distributed pores and increased interface roughness in magnetron sputtered, nanoscale reactive multilayers.[36–39] Although no attempt has yet been made to specifically manipulate the layer morphology of reactive multilayers by laser structuring the substrate, the process-related superimposed roughness would very likely have a negative impact on the layer growth. However, controlling the size and area distribution of the surface topography variations could introduce large area variations in film morphology.

The range of options for complementary post-processing of structured surfaces is limited. Mechanical polishing is only able to process and smoothen the profile tips, while neglecting the valleys.[40] As a result, the overall profile shape is altered, shifting away from, for instance, a sinusoidal surface profile toward plateau-like profile maxima. Müller et al. chemically post-processed laser-patterned copper substrates by immersion etching in 3 % citric acid, and they were able to remove the surface oxides generated during the DLIP process.[14] Although this resulted into a reduced roughness in the area of the profile peaks, there was still a superimposed basic roughness on the surface profile.

In this context, electropolishing emerges as a valuable step in the fabrication process, capable of smoothing surfaces by evenly removing undesired by-products and enhancing their functional characteristics.[41] Since electropolishing is a selective surface treatment method that preferentially removes material from nano- and microscopic sharp profile peaks (due to increased electric field strength) on the surface, it is also capable of smoothing complex geometries, including intricate patterns or irregular shapes.[42–47] Unlike mechanical methods, electropolishing is a non-abrasive process, reducing the risk of introducing defects or microcracks, preserving the integrity of the material. Furthermore, this surface finishing method not only smoothens the surface but also effectively removes contaminants, oxides, and other impurities from the substrate. The result is a cleaner surface with improved corrosion resistance and biocompatibility. This is particularly advantageous in applications such as medical devices or aerospace components.[48]

In this study, we investigated the effectiveness of electropolishing as a post-processing method for DLIP-treated copper surfaces. Through systematic characterization and analysis, we evaluated the impact of electropolishing on the topography, roughness, and structural integrity of the patterned surfaces.

2. Results and Discussion

2.1. Morphological Characterization of DLIP-Treated Samples

An overview of the DLIP-treated samples and their respective structure depths, represented by the mean height of the roughness profile element R_c, is shown in **Table 1**. A detailed description of the sample nomenclature can be found in Section 4. The structure depth consistently increases with the application of a higher accumulated fluence F_{acc} for each structure period.

The laser-processed samples, based on two-beam interference, exhibit a homogeneous wave-like surface profile, as illustrated in **Figure 1**a,c. The examination of the cross-sectional cuts (Figure 1b,d) reveals the presence of a superimposed roughness, which might be unfavorable for the aforementioned potential applications. This superimposed roughness is identified as being primarily caused by highly porous oxide layers, with a heightened prominence in the topographic maxima of the pattern. In picosecond pulsed laser systems, the DLIP process involves the formation of a periodic surface pattern through the combined mechanisms of ablation and redeposition of material.[27] As a result, porous oxide layers are generated on top of the topographic maxima. Furthermore, while the topographic minima are formed by material ablation at the points of maximum intensity, the original surface at the maxima remains unaffected, though concealed beneath the oxide and redeposited material.

Oxidation is expected to occur within the emerging plasma and during material transport.[49] The amount of oxide produced

Table 1. Overview of the DLIP-treated samples, with the structure period P, R_c as a value for the mean structure depth, and the accumulated fluence F_{acc}.

Sample	P [μm]	R_c [μm]	F_{acc} [J cm^{-2}]
2s-ap	2	1.34 ± 0.04	20.88
2d-ap	2	1.88 ± 0.05	41.77
8s-ap	8	2.61 ± 0.07	22.43
8d-ap	8	4.45 ± 0.2	38.41

 © 2024 The Author(s). Advanced Engineering Materials published by Wiley-VCH GmbH

15272648, 2025, 3, Downloaded from https://advanced.onlinelibrary.wiley.com/doi/10.1002/adem.202400435 by Universitätsbibliothek der Universität des Saarlandes, Wiley Online Library on [14/03/2025]. See the Terms and Conditions (https://onlinelibrary.wiley.com/terms-and-conditions) on Wiley Online Library for rules of use; OA articles are governed by the applicable Creative Commons License

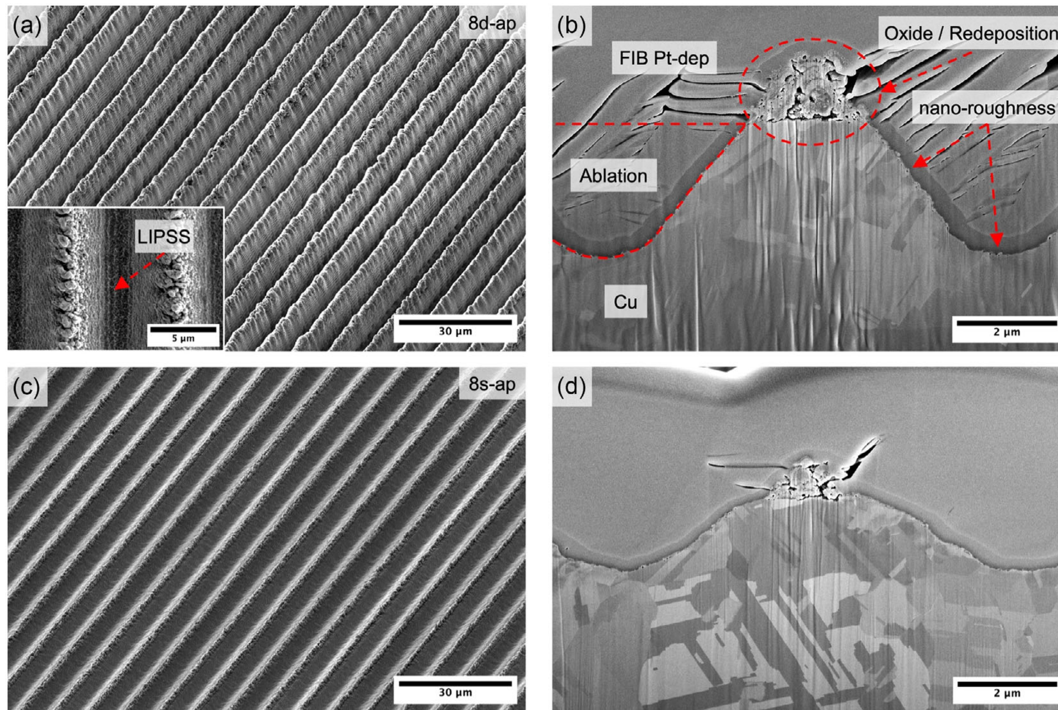

Figure 1. SEM images of DLIP-treated samples with 8 µm periodicity. a,c) Top-down overview micrographs (45° tilt) of 8d-ap and 8s-ap, respectively. b,d) Corresponding cross-sectional view (52° tilt) revealing the morphology of the patterned copper surfaces.

raises with increasing accumulated fluence in agreement with the findings of Fox et al.[50] The structure flanks and topographic minima are less affected. Furthermore, as illustrated in the inset in Figure 1a, LIPSS are generated with periods in the range of the laser's wavelength (532 nm) and an orientation parallel to the line structures. These substructures, combined with minor amounts of oxides, are primarily responsible for the nanoscale roughness at the structure flanks and minima.

2.2. Temporal Evolution of the Surface Characteristics

Following the morphological characterization of the initial state of the laser-structured samples, this section analyzes the temporal evolution of the surfaces during electropolishing. In a first step, focused ion beam (FIB)/scanning electron microscopy (SEM) cross-sections of the laser-structured samples were prepared. The evolution of the surfaces during electropolishing was qualitatively analyzed, starting from the state after laser treatment. In a second step, a semi-quantitative chemical characterization of the individual sample states was carried out using energy-dispersive X-ray spectroscopy (EDS) in FIB/SEM, with a special focus on the morphological features assumed to have the most impact on the surface topography. Finally, a detailed topographic analysis was conducted on the processed surfaces and compared to samples with equivalent structural depths.

2.2.1. Topography Evolution During Electropolishing

Figure 2 exemplifies the evolution of the surfaces over time through electropolishing for sample 8d. The electropolishing process can be divided into two main steps. First, the top part of the topographic maxima, which mainly contains oxides (Figure 2a), is dissolved in the electrolyte after a short period of time (Figure 2b). This leads to an increased load-bearing capacity of the surface, which can be particularly beneficial for tribological applications.[25] In the subsequent step, the sharp, prominent edges at the transition between maxima and minima are rounded due to locally higher current densities, resulting in a smoother surface profile.[41] This process continues until a nearly perfect sinusoidal surface profile is achieved, and the superimposed roughness is eliminated (Figure 2c–e). Consequently, the aspect ratio (AR) is also reduced.

2.2.2. Semi-Quantitative Chemical Analysis

Based on the previous sections, the increased roughness at the topographic maxima is mainly due to oxide formation and redeposited material during laser processing. On the other hand, the formation of LIPSS and smaller amounts of oxides determine the surface topography at the structure flanks and topographic minima. Therefore, a semi-quantitative chemical comparison was conducted between the laser-structured samples and the electropolished samples using EDS with a low acceleration voltage (5 kV) to ensure near-surface measurements and good sensitivity for light elements, particularly oxygen (**Figure 3**).

Figure 3a displays the EDS spectra of sample type 8d. The sample "flat" refers to an unstructured, electropolished copper foil used as a reference. The spectra were normalized to the Cu L_{α} peak to allow for a semi-quantitative comparison. The C K_{α} (≈0.28 keV), O K_{α} (≈0.53 keV), and Cu L_{α} (≈0.93 keV) peaks were detected for every condition. The peak at ≈1.86 keV

 © 2024 The Author(s). Advanced Engineering Materials published by Wiley-VCH GmbH

15272648, 2025, 3, Downloaded from https://advanced.onlinelibrary.wiley.com/doi/10.1002/adem.202400435 by Universitätsbibliothek der Universität des Saarlandes, Wiley Online Library on [14/03/2025]. See the Terms and Conditions (https://onlinelibrary.wiley.com/terms-and-conditions) on Wiley Online Library for rules of use; OA articles are governed by the applicable Creative Commons License

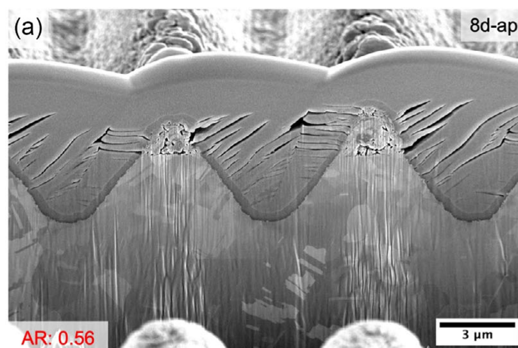

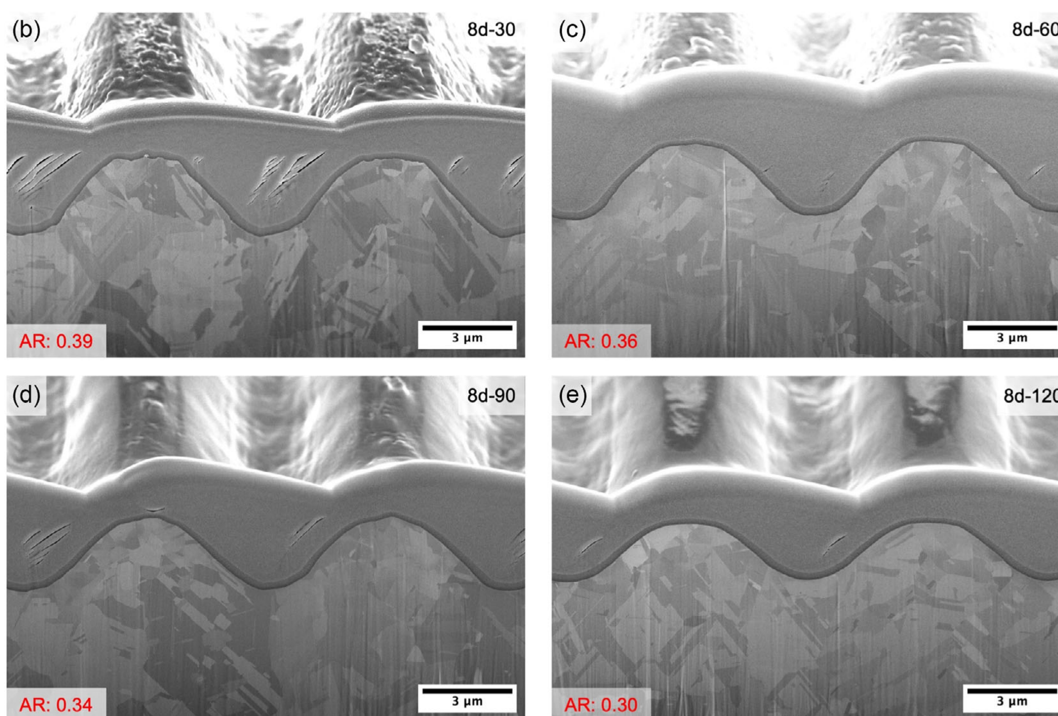

Figure 2. FIB/SEM cross sections (52° tilt) of sample 8d a) before and b–e) after 30, 60, 90, and 120 s of electropolishing.

corresponds to the copper sum peak and occurs when two photons with equal energy hit the detector simultaneously. No phosphorus signal (P $K_\alpha \approx 2.01$ keV) was found in the electropolished samples within the detection limit of the technique, indicating an effective removal of the electrolyte in the cleaning process. Examining the individual oxygen peaks (Figure 3b), a significant decrease in peak height over time is observed. The peak shows its greatest reduction in intensity after only 30 s of electropolishing. This finding confirms the observation made in the previous section that most of the oxide dissolves in the electrolyte after a short period of electropolishing (Figure 2b). With prolonged electropolishing, the signal continues to decrease, but only to a small extent. In this regime, mainly shaping of the structure profile and smoothing of the surface takes place. As a side effect the AR decreases. Only the unstructured, electropolished reference sample "flat" exhibits a lower oxygen signal.

In addition to the full-area spectra, EDS line scans were measured across ten topographic maxima of both as-processed samples and 120 s electropolished samples. The results of 8d-ap and 8d-120 are exemplarily shown and compared in Figure 3c,d, respectively. Large fluctuations in the copper and oxygen signal are present after laser processing. In the peaks of the profile, the copper signal exhibits a local minimum, whereas the oxygen signal reaches its maximum. Conversely, in the valleys, the opposite is observed. The fluctuations in signal intensity can be attributed to two factors. First, the low acceleration voltage of 5 kV results in a lower penetration depth and consequently shallow information depth. Second, oxide formation mainly occurs at

© 2024 The Author(s). Advanced Engineering Materials published by Wiley-VCH GmbH

15272648, 2025, 3, Downloaded from https://advanced.onlinelibrary.wiley.com/doi/10.1002/adem.202400435 by Universitätsbibliothek der Universität des Saarlandes, Wiley Online Library on [14/03/2025]. See the Terms and Conditions (https://onlinelibrary.wiley.com/terms-and-conditions) on Wiley Online Library for rules of use; OA articles are governed by the applicable Creative Commons License

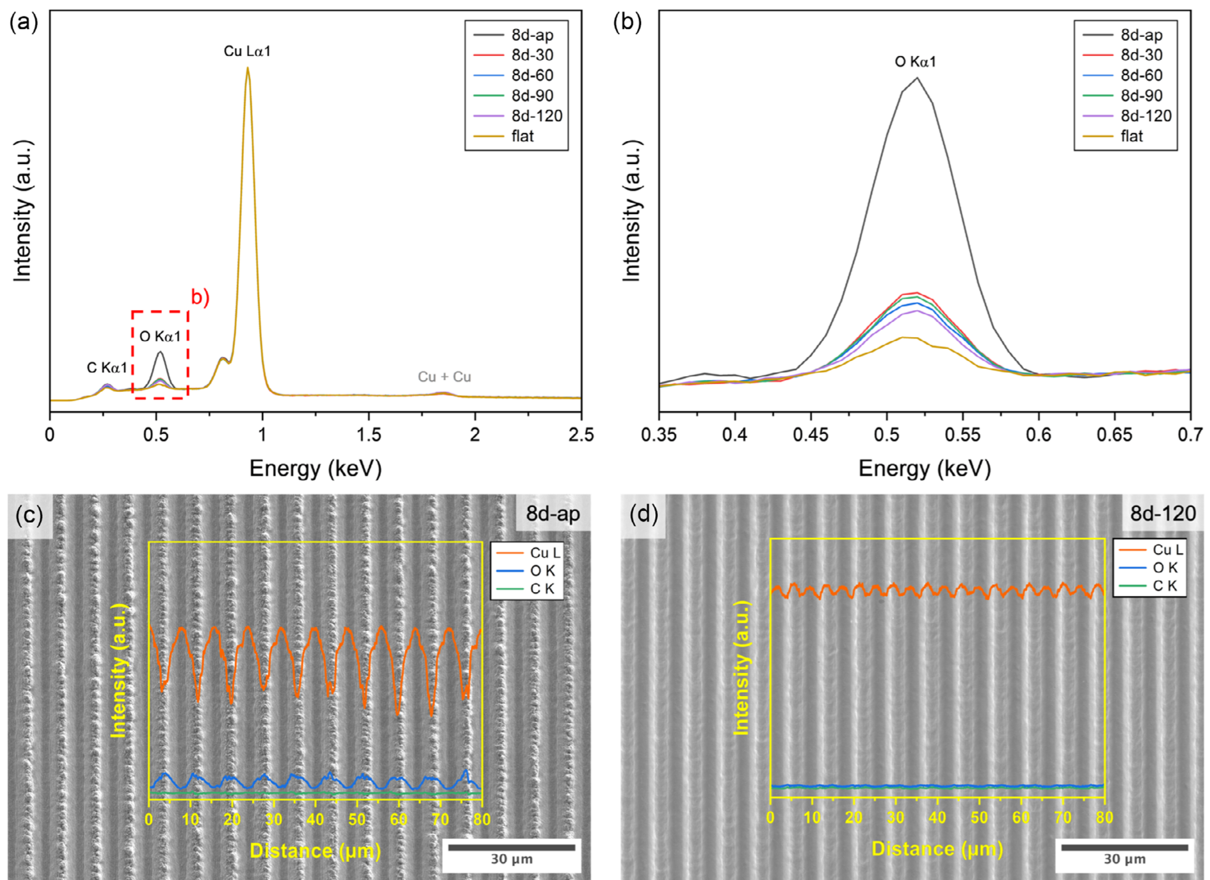

Figure 3. EDS measurements of sample type 8d. a) Comparison of spectra normalized to the Cu L_α peak and b) scaled O K_α signal. O K_α intensity decreases with increasing duration of electropolishing. The EDS line scans across ten neighboring topographic maxima for c) 8d-ap and d) 8d-120 reveal that initially most of the oxide is present on top of the maxima. After electropolishing the oxygen signal flattens out.

the profile peaks, where it covers the copper bulk material, leading to a relative decrease in copper signal intensity compared to the topographic minima, where nearly no oxide is present. After electropolishing, the signal fluctuations for copper decrease significantly. Furthermore, the curve for oxygen levels off, indicating a uniform distribution of oxygen. As a result, oxides are no longer significant from a topographic perspective (see Figure 2).

2.3. Topographic Comparison—DLIP vs DLIP + Electropolishing

To enable a thorough topographic analysis of the laser-structured and subsequently electropolished samples, a reference sample batch with equivalent structure depths was processed without electropolishing. **Table 2** provides an overview of the samples investigated in this section. The structure depths (R_c) of the reference samples were almost identical to those of the laser processed and additionally electropolished samples. Note that the accumulated fluences for the electropolished samples refer to their as-processed state before electropolishing.

Figure 4 shows color-coded height images of the sample type 8s obtained with confocal laser scanning microscopy (CLSM). The images include three profile lines: one along a topographic maximum, one along a topographic minimum, and one across the lines. The profile lines are noticeably smoother for 8s-120 (Figure 4b) than for 8s-ref (Figure 4a), particularly along the topographic maximum. The reduction in superimposed roughness at the maximum can be attributed to the oxide layer removed by electropolishing. This is evident when examining the profiles

Table 2. Sample overview for topographic comparison. Reference samples (only DLIP) show nearly identical structure depths (R_c) as the laser-structured and subsequently electropolished samples.

Sample	P [µm]	R_c [µm]	F_{acc} [J cm^{-2}]
2s-120	2	0.28 ± 0.01	20.88[a)]
2s-ref	2	0.24 ± 0.01	9.28
2d-120	2	0.51 ± 0.03	41.77[a)]
2d-ref	2	0.48 ± 0.02	12.78
8s-120	8	1.27 ± 0.04	22.43[a)]
8s-ref	8	1.28 ± 0.05	11.56
8d-120	8	2.41 ± 0.03	38.41[a)]
8d-ref	8	2.39 ± 0.08	23.13

[a)]Values refer to as-processed samples (before electropolishing).

 © 2024 The Author(s). Advanced Engineering Materials published by Wiley-VCH GmbH

15272648, 2025, 3, Downloaded from https://advanced.onlinelibrary.wiley.com/doi/10.1002/adem.202400435 by Universitätsbibliothek der Universität des Saarlandes, Wiley Online Library on [14/03/2025]. See the Terms and Conditions (https://onlinelibrary.wiley.com/terms-and-conditions) on Wiley Online Library for rules of use; OA articles are governed by the applicable Creative Commons License

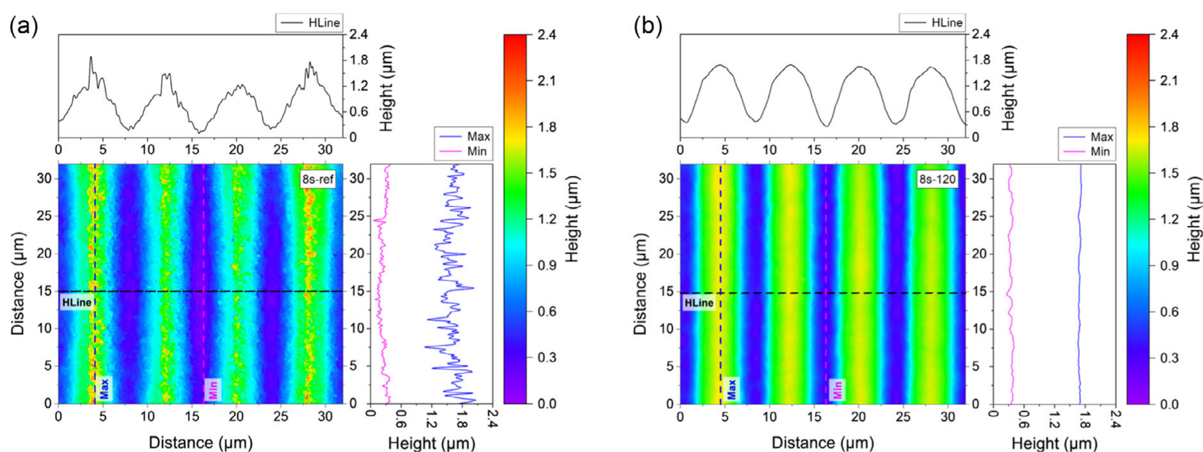

Figure 4. Topographic, color-coded CLSM height images including profile lines along both a topographic maximum and minimum as well as across the line pattern for a) 8s-ref and b) 8s-120.

across the line patterns. The surface profile of 8s-ref exhibits a superimposed roughness, while 8s-120 is characterized by a nearly perfect sinusoidal surface pattern and is considerably more homogeneous in terms of peak/valley distances.

The contrast in surface finish is even more apparent when examining the relevant surface parameters. **Figure 5** shows the color-coded height images of samples 8s-ref (Figure 5a) and 8s-120 (Figure 5b). Furthermore, the root mean square roughness R_q was calculated pixelwise along the line direction (vertical image direction) and superimposed on the height profile images. Along with the arithmetic mean roughness R_a, R_q is the most commonly used parameter to describe the surface quality of technically relevant surfaces. Although R_q is defined similarly to R_a, it is more sensitive to large deviations from the mean line of the surface profile, which is why this value was taken into account when comparing the samples.[51] For 8s-ref, the topographic maxima exhibit an average value of ≈180 nm, which can be attributed to the locally increased amount of porous oxide agglomerations that raise the surface roughness. The sample shows its lowest values for R_q (≈80 nm) in the area of the structural minima. As noted in Section 2.1, the formation of LIPSS with small periods in the range of the laser wavelength and shallow structure depths, as well as smaller amounts of oxides created during the laser process, mainly determine the superimposed roughness in the area of the structure flanks and minima. Consequently, the R_q values are lower in that region. In contrast, 8s-120 (Figure 5b) has the highest values at its structure flanks (≈40–50 nm), while the topographic maxima are markedly smoother (≈20 nm). This is associated to the fact that electropolishing predominantly affects the surface peaks due to locally increased electric field strengths and consequently higher current densities. The flanks and minima are rather faceted through the polishing process (see also Figure 2d,e), resulting in slightly higher roughness values in that area. However, the faceted surfaces are smooth enough to not negatively impact the performance for most potential applications. Additionally, the calculated maximum R_q values for this sample type are still lower than the lowest value of 8s-ref.

Finally, **Figure 6** illustrates two additional parameters for identifying small differences in surface finishes. One of these parameters is the S ratio, which corresponds to the ratio between the real surface area and the projected area (Figure 6a). A smaller

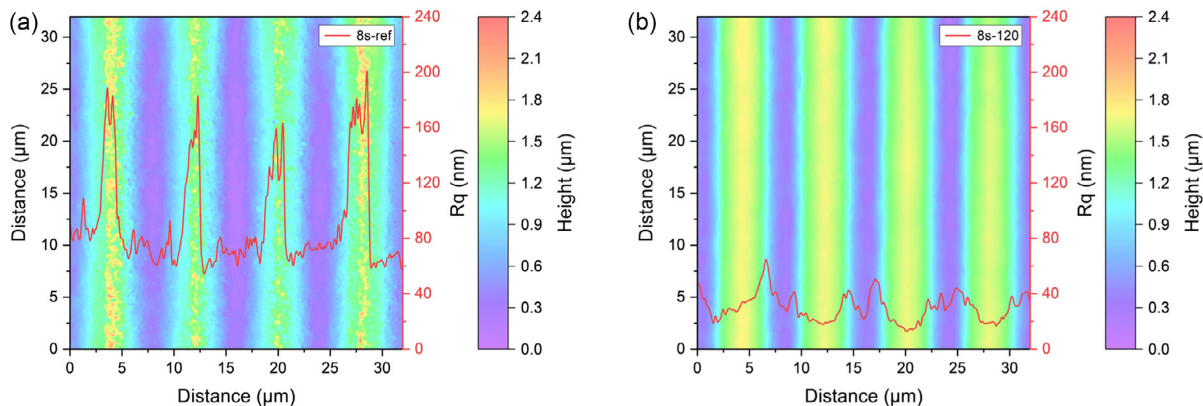

Figure 5. Color-coded CLSM height images of a) 8s-ref and b) 8s-120. In addition, R_q was calculated pixelwise in the vertical image direction (along line pattern).

© 2024 The Author(s). Advanced Engineering Materials published by Wiley-VCH GmbH

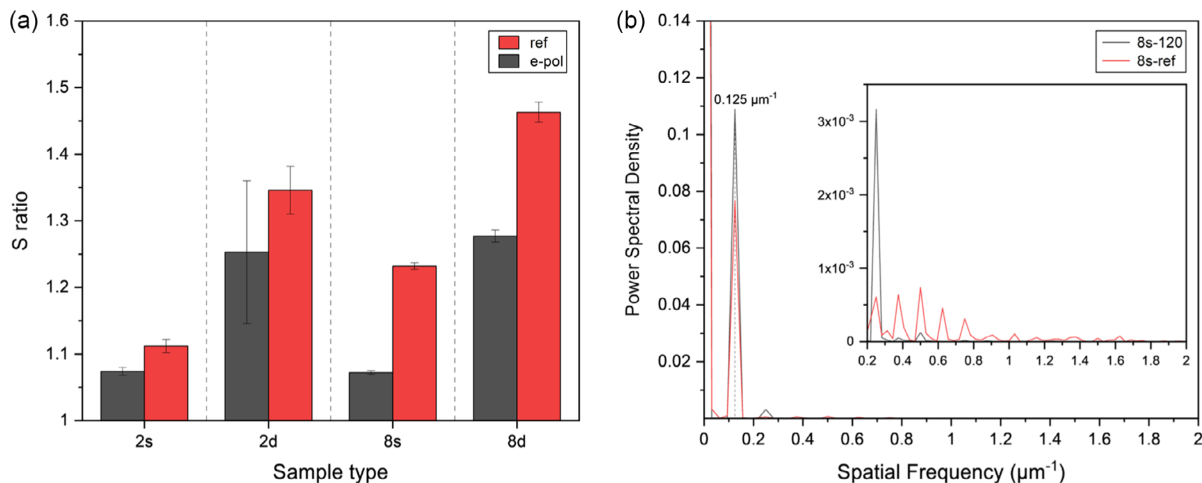

Figure 6. a) Comparison of the S ratio between laser-structured + electropolished samples (e-pol) and only laser-structured reference samples (ref). b) 1D PSD function of 8s-ref and 8s-120.

S ratio indicates a smoother surface finish. Based on the values listed in the diagram, it is evident that the electropolished samples all exhibit a notably smoother surface finish compared with the DLIP-treated reference samples. The most significant differences were observed between the samples with an 8 µm structure period. Electropolishing resulted in a reduction of the *S* ratio by ≈13% compared with the reference in both cases. For the periodicity of 2 µm, the reduction was ≈4% (2s) and 7% (2d).

Another parameter is the power spectral density (PSD) function, which is a useful tool for analyzing and comparing periodic surface profiles, particularly with respect to high-frequency modulations on the surface.[52] The PSD shows the frequency distribution of spatial variations in the topography, providing insights into the surface roughness characteristics of a periodic profile. Figure 6b displays the 1D PSD of 8s-120 and 8s-ref, calculated based on individual profile lines for each. The fundamental frequency (0.125 μm^{-1}) corresponds to the structure period (8 µm), multiples of it to its harmonics. The fundamental peak amplitude is higher for 8s-120, indicating a stronger manifestation of the structure. In the case of sample 8s-ref, the scaled inset in the graph reveals the presence of additional peaks that do not correspond to harmonics, which suggests the formation of a superimposed structure.

3. Conclusion

This study investigated the effectiveness of electropolishing as a post-processing method for DLIP-treated copper surfaces, aiming to address challenges such as surface roughness and non-uniformity. Through systematic characterization and analysis, it was demonstrated that electropolishing effectively smoothens DLIP-treated surfaces by selectively removing undesired by-products such as oxides and redeposited material, thereby enhancing their functional characteristics. The electropolishing process was found to significantly reduce the superimposed roughness of DLIP-patterned surfaces, resulting in smoother surface profiles. This was evidenced by morphological characterization, chemical analysis, and topographic comparison between DLIP-treated samples and samples subjected to DLIP followed by electropolishing. Electropolishing not only improved the surface smoothness but also homogenized the distribution of surface oxides, leading to improved surface quality. Moreover, apart from numerous other potential applications, employing the combination of DLIP and subsequent electropolishing on substrates for sputter deposited reactive multilayers offers a promising avenue to modify the morphology of the deposited layers, altering the reaction characteristics and overall performance of the multilayer system. This underscores the versatility and significance of electropolishing in tailoring surface properties for various technological applications. Further research could explore the optimization of electropolishing parameters for specific DLIP-treated surfaces and investigate the performance of electropolished surfaces in practical applications. Subsequent studies will furthermore investigate the potential for well-defined morphology modification of PVD multilayer thin films.

4. Experimental Section

Material and Pretreatment: Electrodeposited copper foils with a smooth surface profile (R_a = 20 nm ± 1 nm) were purchased from CIRCUIT FOIL (Luxembourg). The chromium-passivated copper foils were cut into (5 × 2.5) cm^2 sheets and had a total thickness of 70 µm. Prior to laser processing, the thin passivation layer (<3 mg m^{-2}) was removed by etching the samples in 10% sulfuric acid for 3 min, immediately followed by immersion in deionized water, and finally cleaning in ethanol for 10 min. Both steps, etching in sulfuric acid and cleaning in ethanol were carried out in an ultrasonic bath. After cleaning, the remaining ethanol was removed from the surface with compressed air.

Direct Laser Interference Patterning: An Edgewave px-series picosecond laser system with a pulse duration of 12 ps, a wavelength of 532 nm, a repetition rate of 100 kHz, and a maximum average power of 10 W was used to modify the surface topography of the samples. Since the general principle of the DLIP technique is based on the interference of two or more laser beams, the main beam leaving the laser head has to be split into several sub-beams which are then overlapped on the sample surface to

© 2024 The Author(s). Advanced Engineering Materials published by Wiley-VCH GmbH

15272648, 2025, 3, Downloaded from https://advanced.onlinelibrary.wiley.com/doi/10.1002/adem.202400435 by Universitätsbibliothek der Universität des Saarlandes, Wiley Online Library on [14/03/2025]. See the Terms and Conditions (https://onlinelibrary.wiley.com/terms-and-conditions) on Wiley Online Library for rules of use; OA articles are governed by the applicable Creative Commons License

15272648, 2025, 3, Downloaded from https://advanced.onlinelibrary.wiley.com/doi/10.1002/adem.202400435 by Universitätsbibliothek der Universität des Saarlandes, Wiley Online Library on [14/03/2025]. See the Terms and Conditions (https://onlinelibrary.wiley.com/terms-and-conditions) on Wiley Online Library for rules of use; OA articles are governed by the applicable Creative Commons License

create the interference pattern. The pattern type depends only on the laser wavelength λ, the angle between the incident beams (2θ), the number of beams interfering on the sample surface, and the polarization of the laser. The resulting structure period P is given by[53]

$$P = \frac{\lambda}{2\sin(\theta)} \tag{1}$$

In this work, the main beam was split into four coherent sub-beams using a diffractive optical element (DOE), as schematically shown in **Figure 7**. The motorized, height-adjustable prism parallelizes the split beams before they are finally superimposed on the sample surface by a focusing lens. The angle of incidence and thus the structure period can be adjusted by changing the distance between the DOE and the prism. By inserting apertures directly above the focusing lens, individual sub-beams can be blanked out. Thus, the desired anisotropic line pattern was achieved by masking two of the four sub-beams.

The pattern periods chosen were 2 and 8 μm, each with two different structure depths, resulting in four different configurations. The process parameters for the targeted structural features, i.e., mainly the structure depth, were calculated according to a routine developed by Fox and Mücklich in a previous work.[54] The optical setup is part of a fully enclosed structuring system (RDX 500nano, Pulsar Photonics) including an x-y-stage.

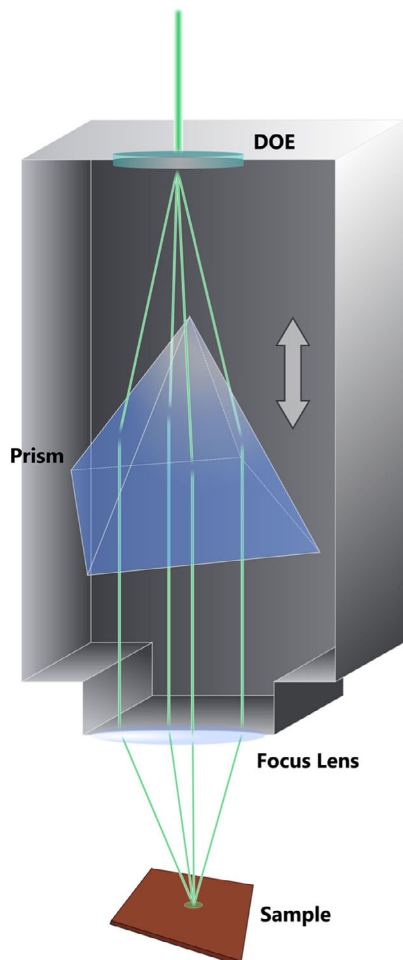

Figure 7. Schematic of the DLIP optics head. The DOE splits the main beam into four sub-beams, which are then parallelized by a height-adjustable prism. The lens below the prism finally focuses the beams on the sample surface.

Electropolishing: The laser-structured copper foils were electropolished in orthophosphoric acid (85%). To preclude the generation of oxygen and thus the preferential occurrence of pitting on the surface of the sample, a voltage of 1.5 V DC was applied in order to ensure polishing within the "limiting current density plateau" region of the corresponding polarization curve.[55,56] The duration of the electropolishing was varied in 30 s steps between 30 s and 2 min to verify the time-dependent topographic evolution of the surface profile during the process ex situ. The copper samples served as the anode, whereas another copper sheet was used as the cathodic counterelectrode (see **Figure 8**). After electropolishing, the samples were immediately rinsed in deionized water followed by cleaning in ethanol for 10 min in an ultrasonic bath to ensure complete removement of the phosphoric acid.

Sample Nomenclature: The different sample types were labeled using the scheme depicted in **Table 3**. As an example, the denotation 8d-90 refers to a sample that was laser-structured with a structure period of 8 μm and a high AR (deeper pattern). Subsequently, the sample was electropolished for 90 s.

Characterization Techniques: The copper surfaces were topographically characterized by CLSM (LEXT OLS4100, Olympus) both after laser treatment and after electropolishing for varying durations. The microscope operated at a laser wavelength of 405 nm. The measurements were taken using a 50× objective (N.A. = 0.95) with different additional zooms, resulting in a lateral and vertical resolution of 120 nm (at 8× zoom) and 10 nm, respectively. SEM

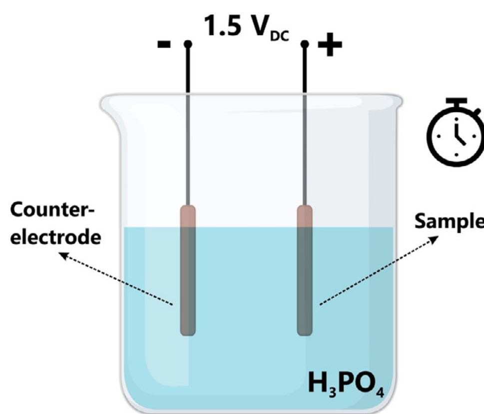

Figure 8. Illustration of the arrangement in the electrolytic cell. The laser-structured copper foils were connected to the positive terminal of a DC voltage source. Another copper plate served as the cathode. Both electrodes were dipped into orthophosphoric acid (85%) as electrolyte.

Table 3. Nomenclature for sample names according to the schema <period><depth>-<condition>.

Parameter	Variations	Description
Structure period P	2	[μm]
	8	
Structure depth	s	Shallow
	d	Deep
Condition	ap	DLIP
	30	DLIP + 30 s electropolishing
	60	DLIP + 60 s electropolishing
	90	DLIP + 90 s electropolishing
	120	DLIP + 120 s electropolishing
	ref	DLIP (aspect ratio ≅ condition 120)

 © 2024 The Author(s). Advanced Engineering Materials published by Wiley-VCH GmbH

cross-sectional images were acquired using a dual-beam Xe-FIB/SEM workstation (Helios G4 PFIB CXe, Thermo Fisher) to qualitatively compare the samples with respect to oxide formation during laser processing and surface profile evolution by electropolishing. EDS spectra and line scans perpendicular to the lines of the patterns were conducted using the integrated EDS detector (EDAX Octane Elite). To minimize shadowing effects caused by the topography of the structures during the measurements, the lines of the patterns were aligned parallel to the detector. Both SEM imaging and EDS measurements were conducted using an acceleration voltage of 5 kV.

Acknowledgements

The authors wish to acknowledge funding from Deutsche Forschungsgemeinschaft (DFG), project number 426339194 and funding for the FIB/SEM instrument Helios G4 PFIB CXe, Thermo Fisher, project number 415217285.

Open Access funding enabled and organized by Projekt DEAL.

Conflict of Interest

The authors declare no conflict of interest.

Data Availability Statement

The data that support the findings of this study are available from the corresponding author upon reasonable request.

Keywords

electropolishing, laser structuring, periodic structures, topography

Received: February 19, 2024
Revised: June 11, 2024
Published online: July 18, 2024

[1] B. Bhushan, *Philos. Trans. R. Soc., A* **2009**, *367*, 1445.
[2] P. G. Grützmacher, F. J. Profito, A. Rosenkranz, *Lubricants* **2019**, *7*, 95.
[3] A. Rosenkranz, L. Reinert, C. Gachot, F. Mücklich, *Wear* **2014**, *318*, 49.
[4] C. Gachot, A. Rosenkranz, S. M. Hsu, H. L. Costa, *Wear* **2017**, *372–373*, 21.
[5] K. E. Trinh, E. Ramos-Moore, I. Green, C. Pauly, M. Zamanzade, F. Mucklich, *IEEE Trans. Compon. Packag. Manuf. Technol.* **2017**, *7*, 582.
[6] S. Schütz, S. Suarez, F. Mücklich, *Tribol. Lett.* **2023**, *71*, 127.
[7] K. E. Trinh, A. Tsipenyuk, M. Varenberg, A. Rosenkranz, N. Souza, F. Mücklich, *Wear* **2015**, *344–345*, 86.
[8] A. I. Aguilar-Morales, S. Alamri, B. Voisiat, T. Kunze, A. F. Lasagni, *Materials* **2019**, *12*, 2737.
[9] S. M. Lößlein, F. Mücklich, P. G. Grützmacher, *J. Colloid Interface Sci.* **2022**, *609*, 645.
[10] A. Fernández, A. Francone, L. H. Thamdrup, A. Johansson, B. Bilenberg, T. Nielsen, M. Guttmann, C. M. Sotomayor Torres, N. Kehagias, *ACS Appl. Mater. Interfaces* **2017**, *9*, 7701.
[11] W. Pfleging, R. Kohler, M. Torge, V. Trouillet, F. Danneil, M. Stüber, *Appl. Surf. Sci.* **2011**, *257*, 7907.
[12] L. Müller-Meskamp, Y. H. Kim, T. Roch, S. Hofmann, R. Scholz, S. Eckardt, K. Leo, A. F. Lasagni, *Adv. Mater.* **2012**, *24*, 906.
[13] M. S. Kim, J. H. Lee, M. K. Kwak, *Int. J. Precis. Eng. Manuf.* **2020**, *21*, 1389.
[14] D. W. Müller, S. Lößlein, E. Terriac, K. Brix, K. Siems, R. Moeller, R. Kautenburger, F. Mücklich, *Adv. Mater. Interfaces* **2021**, *8*, 2001656.
[15] S. Rigo, C. Cai, G. Gunkel-Grabole, L. Maurizi, X. Zhang, J. Xu, C. G. Palivan, *Adv. Sci.* **2018**, *5*, 1700892.
[16] K. Anselme, L. Ploux, A. Ponche, *J. Adhes. Sci. Technol.* **2010**, *24*, 2141.
[17] C. Liang, Y. Hu, H. Wang, D. Xia, Q. Li, J. Zhang, J. Yang, B. Li, H. Li, D. Han, M. Dong, *Biomaterials* **2016**, *103*, 170.
[18] B. Voisiat, W. Wang, M. Holzhey, A. F. Lasagni, *Sci. Rep.* **2019**, *9*.
[19] F. Rößler, T. Kunze, A. F. Lasagni, *Opt. Express* **2017**, *25*, 22959.
[20] A. Jain, V. Bajpai, *Surf. Coat. Technol.* **2019**, *380*, 125087.
[21] A. Szurdak, A. Rosenkranz, C. Gachot, G. Hirt, F. Mücklich, *Key Eng. Mater.* **2014**, *611–612*, 417.
[22] W. Koszela, P. Pawlus, L. Galda, *Wear* **2007**, *263*, 1585.
[23] P. Pawlus, *Tribol. Int.* **1993**, *26*, 49.
[24] U. Pettersson, S. Jacobson, *Tribol. Int.* **2003**, *36*, 857.
[25] C. Schäfer, L. Reinert, T. MacLucas, P. Grützmacher, R. Merz, F. Mücklich, S. Suarez, *Tribol. Lett.* **2018**, *66*, 89.
[26] D. W. Müller, T. Fox, P. G. Grützmacher, S. Suarez, F. Mücklich, *Sci. Rep.* **2020**, *10*, 3647.
[27] A. F. Lasagni, C. Gachot, K. E. Trinh, M. Hans, A. Rosenkranz, T. Roch, S. Eckhardt, T. Kunze, M. Bieda, D. Günther, V. Lang, F. Mücklich, in *Proc. SPIE* **2017**, 1009211.
[28] J. Bonse, J. Krüger, S. Höhm, A. Rosenfeld, *J. Laser Appl.* **2012**, *24*, 420061.
[29] T. T. D. Huynh, A. Petit, N. Semmar, *Appl. Surf. Sci.* **2014**, *302*, 109.
[30] Y. F. Gao, C. Y. Yu, B. Han, M. Ehrhardt, P. Lorenz, L. F. Xu, R. H. Zhu, *Surf. Interfaces* **2020**, *19*, 100538.
[31] C. Florian, S. V. Kirner, J. Krüger, J. Bonse, *J. Laser Appl.* **2020**, *32*, 022063.
[32] P. Gregorčič, M. Sedlaček, B. Podgornik, J. Reif, *Appl. Surf. Sci.* **2016**, *387*, 698.
[33] A. Rudenko, C. Mauclair, F. Garrelie, R. Stoian, J. P. Colombier, *Nanophotonics* **2019**, *8*, 459.
[34] P. G. Slade, *Electrical Contacts: Principles and Applications*, CRC Press, Boca Raton, FL **2014**.
[35] P. Panjan, A. Drnovšek, P. Gselman, M. Čekada, M. Panjan, *Coatings* **2020**, *10*, 447.
[36] K. Jaekel, Y. Sauni Camposano, S. Matthes, M. Glaser, P. Schaaf, J. Bergmann, J. Mueller, H. Bartsch, *J. Mater. Sci.* **2023**, *58*, 12811.
[37] Y. H. Sauni Camposano, S. S. Riegler, K. Jaekel, J. Schmauch, C. Pauly, C. Schäfer, H. Bartsch, F. Mücklich, I. Gallino, P. Schaaf, *Appl. Sci.* **2021**, *11*, 9304.
[38] B. Liu, X. Yu, X. Jiang, Y. Qiao, L. You, Y. Wang, F. Ye, *Appl. Surf. Sci.* **2021**, *546*, 149098.
[39] Y. H. Sauni Camposano, H. Bartsch, S. Matthes, M. Oliva-Ramirez, K. Jaekel, P. Schaaf, *Phys. Status Solidi A* **2023**, *220*, 2200765.
[40] P. G. Grützmacher, A. Rosenkranz, A. Szurdak, M. Grüber, C. Gachot, G. Hirt, F. Mücklich, *Ind. Lubr. Tribol.* **2019**, *71*, 1007.
[41] S. Zaki, N. Zhang, M. D. Gilchrist, *Micromachines* **2022**, *13*, 468.
[42] D. Berestovskyi, W. N. P. Hung, P. Lomeli, *J. Micro Nano-Manuf.* **2014**, *2*, 041005.
[43] S. Kissling, K. Bade, M. Börner, D. M. Klymyshyn, *Microsyst. Technol.* **2010**, *16*, 1361.
[44] E. Kassab, A. Marquardt, L. Neelakantan, M. Frotscher, F. Schreiber, T. Gries, S. Jockenhoevel, J. Gomes, G. Eggeler, *Materialwiss. Werkstofftech.* **2014**, *45*, 920.
[45] J. Kim, J. K. Park, H. K. Kim, A. R. Unnithan, C. S. Kim, C. H. Park, *J. Nanosci. Nanotechnol.* **2017**, *17*, 2333.
[46] P. Sojitra, C. Engineer, D. Kothwala, A. Raval, H. Kotadia, G. Mehta, *Trends Biomater. Artif. Organs* **2010**, *23*, 115.
[47] P. Pendyala, M. S. Bobji, G. Madras, *Tribol. Lett.* **2014**, *55*, 93.
[48] W. Han, F. Fang, *Int. J. Mach. Tools Manuf.* **2019**, *139*, 1.
[49] C. Zwahr, R. Helbig, C. Werner, A. F. Lasagni, *Sci. Rep.* **2019**, *9*.
[50] T. Fox, P. Maria Delfino, F. Cortés, C. Pauly, D. Wyn Müller, M. Briesenick, G. Kickelbick, F. Mücklich, *ChemNanoMat* **2023**, *9*, e202300314.
[51] E. S. Gadelmawla, M. M. Koura, T. M. A. Maksoud, I. M. Elewa, H. H. Soliman, *J. Mater. Process. Technol.* **2002**, *123*, 133.

 © 2024 The Author(s). Advanced Engineering Materials published by Wiley-VCH GmbH

15272648, 2025, 3, Downloaded from https://advanced.onlinelibrary.wiley.com/doi/10.1002/adem.202400435 by Universitätsbibliothek der Universität des Saarlandes, Wiley Online Library on [14/03/2025]. See the Terms and Conditions (https://onlinelibrary.wiley.com/terms-and-conditions) on Wiley Online Library for rules of use; OA articles are governed by the applicable Creative Commons License

[52] Y. Gong, S. T. Misture, P. Gao, N. P. Mellott, *J. Phys. Chem. C* **2016**, *120*, 22358.
[53] A. Lasagni, M. D'Alessandria, R. Giovanelli, F. Mücklich, *Appl. Surf. Sci.* **2007**, *254*, 930.
[54] T. Fox, F. Mücklich, *Adv. Eng. Mater.* **2022**, *25*, 2201021.
[55] Y. F. Wu, T. H. Tsai, J. Y. Lin, *Int. J. Electrochem. Sci.* **2019**, *14*, 11035.
[56] G. Yang, B. Wang, K. Tawfiq, H. Wei, S. Zhou, G. Chen, *Surf. Eng.* **2017**, *33*, 149.

 © 2024 The Author(s). Advanced Engineering Materials published by Wiley-VCH GmbH

15272648, 2025, 3, Downloaded from https://advanced.onlinelibrary.wiley.com/doi/10.1002/adem.202400435 by Universitätsbibliothek der Universität des Saarlandes, Wiley Online Library on [14/03/2025]. See the Terms and Conditions (https://onlinelibrary.wiley.com/terms-and-conditions) on Wiley Online Library for rules of use; OA articles are governed by the applicable Creative Commons License